A role for yeast oxysterol-binding protein homologs in endocytosis and in the maintenance of intracellular sterol-lipid distribution

Christopher T. Beh*,‡ and Jasper Rine

Department of Molecular and Cell Biology, University of California, 401 Barker Hall, Berkeley, CA 94720, USA
*Present address: Department of Molecular Biology and Biochemistry, 8888 University Drive, Simon Fraser University, Burnaby, BC V5A 1S6, Canada
‡Author for correspondence (e-mail: ctbeh@sfu.ca)

Accepted 12 February 2004
Journal of Cell Science 117, 2983-2996 Published by The Company of Biologists 2004
doi:10.1242/jcs.01157

Summary

The seven yeast *OSH* genes (*OSH1-OSH7*) encode a family of orthologs of the mammalian oxysterol-binding protein (OSBP). The *OSH* genes share at least one essential overlapping function, potentially linked to the regulation of secretory trafficking and membrane lipid composition. To investigate the essential roles of the *OSH* genes, we constructed conditional *OSH* mutants and analyzed their cellular defects. Elimination of all *OSH* function altered intracellular sterol-lipid distribution, caused vacuolar fragmentation, and resulted in an accumulation of lipid droplets in the cytoplasm and within vacuolar fragments. Gradual depletion of Osh proteins also caused cell budding defects and abnormal cell wall deposition. In *OSH* mutant cells endocytosis was severely impaired, but protein transport to the vacuole and the plasma membrane was largely unaffected. Other mutants affecting sterol-lipid function and distribution, namely *erg2*Δ and *arv1*Δ, shared similar defects. These findings suggested that *OSH* genes, through effects on intracellular sterol distribution, establish a plasma membrane lipid composition that promotes endocytosis.

Key words: OSBP, *OSH* genes, Intracellular lipid transport, Endocytosis, Ergosterol

Introduction

Sterol lipids, such as cholesterol and the fungal sterol ergosterol, are essential for plasma membrane integrity and structure. Changes in sterol levels and composition have extensive effects on membrane function. Ergosterol is important for yeast membrane structure, but it also influences membrane dynamics and the activities of membrane proteins (Gaber et al., 1989; Welihinda et al., 1994). Perturbations in cellular ergosterol and sterol lipid levels affect yeast cell fusion during mating (Gaber et al., 1989; Tomeo et al., 1992), vacuolar homotypic membrane fusion (Kato and Wickner, 2001), and secretory transport to the cell surface (Hardwick and Pelham, 1994; Bagnat et al., 2000). Yeast endocytosis is particularly sensitive to sterol composition (Munn et al., 1999).

Cholesterol and yeast ergosterol are both primarily localized in the plasma membrane. To maintain constant levels, these sterols are specifically transported to the plasma membrane from their site of synthesis in the endoplasmic reticulum (ER). Once in the plasma membrane, cholesterol and ergosterol are recycled back to the plasma membrane if internalized into the cell after endocytosis. In animals, cholesterol is delivered to the plasma membrane by at least two different transport pathways. Cholesterol transport can follow either the established pathway for glycoprotein secretion, or an undefined nonvesicular transport pathway (Kaplan et al., 1985; Urbani et al., 1990; Heino et al., 2000). Pathways for recycling internalized sterols back to the plasma membrane after endocytosis are poorly understood.

Oxysterol-binding proteins (OSBPs) constitute a conserved family of lipid-binding proteins that are implicated in the maintenance of sterol and sphingolipid composition in membranes (Dawson et al., 1989; Jiang et al., 1994; Ridgway et al., 1998; Storey et al., 1998; Beh et al., 2001). The canonical mammalian OSBP was identified based on its high affinity for oxysterols, which are oxygenated derivatives of sterols (Taylor et al., 1984). Oxysterols, such as 25-hydroxycholesterol, are more potent than cholesterol itself as feedback regulators of sterol synthesis, suggesting that they are the sterol metabolites whose levels control the de novo synthesis of sterols (Kandutsch et al., 1978). These findings implied that OSBPs mediate the effects of oxysterols, and OSBPs were once considered candidates for regulators of sterol synthesis feedback control (Taylor et al., 1984). However, other proteins are now known to mediate feedback regulation (Brown and Goldstein, 1997; Brown and Goldstein, 1999) and recent data point to other sterol-related regulatory roles for OSBP and its homologs.

The exact function of the OSBP protein family is unknown, but genetic analysis of the seven yeast OSBP orthologs (the *OSH* genes) affirmed that OSBPs are involved in some aspect of sterol regulation (Jiang et al., 1994; Beh et al., 2001). Although none of the *OSH* genes encodes an essential product, the elimination of the entire *OSH* gene family is lethal (Beh et al., 2001). When all seven Osh proteins are depleted from yeast, a drastic change in cellular sterol composition results and ergosterol levels increase by 3.5-fold (Beh et al., 2001). These findings indicate that the *OSH* gene family shares at least

one essential overlapping function, potentially linked to sterol regulation. As part of the genetic analysis of the *OSH* genes, all 127 possible combinations of *OSH* deletion alleles were constructed and 125 of these combinations were in fact viable (Beh et al., 2001). Many of these viable *OSH* deletion combinations were characterized by specific sterol and membrane defects. These results underscore the regulatory link between Osh proteins and sterol lipids.

The effects of Osh proteins are not restricted to sterols but also include phospholipids. Several Osh proteins have been demonstrated to bind directly to phosphoinositide lipids (Levine and Munro, 1998; Li et al., 2002). Many of these Osh proteins also bind Scs2p, a yeast VAP (VAMP-associated protein) homolog that appears to recruit a variety of known phospholipid regulators to the ER membrane (Loewen et al., 2003). This is a conserved interaction because mammalian OSBP and VAP also physically interact (Wyles et al., 2002). Another regulator of lipid metabolism, encoded by *SEC14*, genetically interacts with *OSH4*. *SEC14* encodes a phospholipid transfer protein, which creates a membrane lipid composition that promotes Golgi-derived secretory transport (Bankaitis et al., 1990). The deletion of *OSH4*/*KES1*, but none of the other *OSH*s, bypasses the essential requirement for *SEC14* (Fang et al., 1996; Beh et al., 2001). This indicates that this *SEC14* interaction is specific to *OSH4*, and that *OSH4* is a negative regulator of *SEC14*-dependent secretion. The implication of these studies is that yeast Osh proteins are recruited to specific compartments together with other lipid regulators to adjust local lipid composition and, thereby, to influence membrane dynamics. Specifically how this mechanism might affect normal cellular functions is not yet understood.

In this paper, we investigated the role of the *OSH* gene family in cell growth to determine cellular processes that are dependent on all *OSH* genes. Our data indicated that the *OSH*s are required for regulating cellular sterol-lipid distribution, and for maintaining plasma membrane and vacuolar morphology. Daughter cell budding was defective in yeast depleted of Osh proteins, and lipid droplets and sterol lipids accumulated within cells. We found that endocytosis was disrupted in *OSH* mutants and also in other previously described mutants that perturb ergosterol distribution within cells. These findings established that, collectively, the yeast *OSH* gene family facilitates bud formation, endocytosis and affects intracellular sterol distribution.

Materials and Methods

Strains, microbial and genetic techniques

Culture media and genetic manipulations were as described (Adams et al., 1997). To select for the *kan*-MX4 gene, yeast were grown on yeast rich medium (YPD) containing 200 μg ml^{-1} geneticin sulfate (G418) (Gibco BRL Life Technologies, Rockville, MD) (Wach et al., 1994).

Yeast strains used in this study are listed in Table 1. The seven *OSH* genes, *OSH1-OSH7*, corresponded to the open reading frames YAR042w, YDL019c, YHR073w, YPL145c, YOR237w, YKR003w and YHR001w, respectively. *OSH1* is a fusion of the open reading frames previously designated YAR042w and YAR044w in the completed yeast genome sequence (Schmalix et al., 1994; Goffeau et al., 1996; Beh et al., 2001; Levine et al., 1998; Levine et al., 2001).

Cloning and gene disruptions

DNA cloning techniques and bacterial transformations were performed by standard procedures (Sambrook et al., 1989). Restriction enzymes were obtained from New England Biolabs (Beverly, MA). Oligonucleotide primers for polymerase chain reaction (PCR) were purchased from Operon Technologies (Alameda, CA).

To disrupt the *VPS4* gene in SEY6210, a fragment containing *vps4*Δ::*kan-MX4* with flanking sequences amplified by PCR was used for one-step gene replacement (Adams et al., 1997). The *vps4*Δ disruption fragment was amplified from genomic DNA derived from a S288C *vps4*Δ::*kan-MX4* strain (Research Genetics, Huntsville, AL) (Winzeler et al., 1999) and used as a template with the oligonucleotide primer combination: 5′-GTCCGATTCACATGTCGCCACTCC-3′ and 5′-CAAGCCGAATTGAACCAAATGAGCGC-3′.

To subclone the wild-type *OSH4*/*KES1* gene, a 2.4 kb *Sac*I-*Cla*I *OSH4*/*KES1* genomic fragment was inserted into the complementary sites of pRS316, a *URA3*-marked *ARS*/*CEN* plasmid (Sikorski and Hieter, 1989) thereby generating pCB231.

OSH4/KES1 plasmid mutagenesis

To generate conditional mutant alleles of *OSH4*/*KES1*, pCB231 was mutagenized in vitro with hydroxylamine as described previously (Adams et al., 1997), and transformed into JRY6326, a strain whose growth on methionine-containing medium requires *OSH* function (Beh et al., 2001). From independent pools of mutagenized plasmids transformed into yeast, two transformants were isolated that rescued JRY6326 methionine-sensitivity at 23°C, but not 37°C. The fragments containing these two temperature-sensitive alleles, *osh4-1* and *osh4-2*, and the wild-type *OSH4*/*KES1* gene, were each subcloned into pRS314, a *TRP1*-marked *ARS*/*CEN* plasmid (Sikorski and Hieter, 1989), generating the plasmids pCB255, pCB256 and pCB254 respectively. At 23°C, these plasmids conferred growth to yeast devoid of all *OSH* genes but at 37°C, only transformants containing the plasmid with wild-type *OSH4*/*KES1* grew.

Filipin/sterol fluorescence microscopy

To examine sterol-lipid distribution using filipin, 1 ml 37.5% formaldehyde was added to 9 ml of cell culture grown in synthetic medium to a density of 0.7 OD_{600} units ml^{-1} (early midlog). After 10 minutes of constant mixing at 23°C, the fixed cells were centrifuged and the pellet was washed twice with 10 ml distilled water. The washed cells were resuspended in 1 ml of water from which 0.2 ml was mixed with 4 μl of freshly made 5 mg ml^{-1} filipin complex (Sigma Chemical, St Louis, MO) in ethanol (on ice). After incubating in the dark with filipin for 15 minutes at 23°C, cells were spotted directly on slides and filipin fluorescence was observed with a UV filter set using neutral density filters.

For all fluorescence microscopy, samples were mounted on poly-lysine coated slides, sealed under coverslips with nail polish, and imaged on an Eclipse E600 microscope (Nikon, Tokyo, Japan) equipped with a CCD digital camera (Hamamatsu Phototonics, Hamamatsu-City, Japan).

Lucifer yellow uptake assay

Fluid-phase endocytosis was observed in 2.5 OD_{600} units of cells harvested from cultures grown in synthetic medium at 23°C to a density of 0.25 OD_{600} units ml^{-1}. Cells were resuspended in 200 μl of synthetic medium and split into two samples. One sample was incubated for 60 minutes at 37°C, the other for 60 minutes at 23°C, prior to the addition of 50 μl 40 mg ml^{-1} lucifer yellow CH (Sigma Chemicals). After lucifer yellow addition, the samples were incubated at the same temperatures for an additional 120 minutes. The cells were then centrifuged and pellets were washed three times with 200 μl ice-cold 50 mM succinic acid, 20 mM NaN_3 pH 5.0 and resuspended in 30 μl of the same buffer before viewing by fluorescence microscopy.

Table 1. Yeast strains used

Strain	Genotype	Origin*
CBY340	MAT**a** *ura3-52 his3Δ200 lys2-801 leu2-3, 112 trp1Δ901 suc2Δ9*	
CBY678	MATα *ura3Δ0 leu2Δ0 lys2Δ0 his3Δ1 met15Δ0 erg2Δ::kan-MX4*	
CBY745	MATα *ura3Δ0 leu2Δ0 lys2Δ0 erg9Δ::kan-MX4 HIS3::*P^{MET3}*-ERG9*	
CBY824	*SEY6210 vps4Δ::kan-MX4*	
CBY858	MATα *ura3Δ0 leu2Δ0 lys2Δ0 his3Δ::kan-MX4*	
CBY886	*SEY6210 osh1Δ::kan-MX4 osh2Δ::kan-MX4 osh3Δ::LYS2 osh4Δ::HIS3 osh5Δ::LEU2 osh6Δ::LEU2 osh7Δ::HIS3* [*osh4-1, URA3*]	
CBY892	*SEY6210 osh1Δ::kan-MX4 osh2Δ::kan-MX4 osh3Δ::LYS2 osh4Δ::HIS3 osh5Δ::LEU2 osh6Δ::LEU2 osh7Δ::HIS3* [*osh4-2, URA3*]	
CBY924	*SEY6210 osh1Δ::kan-MX4 osh2Δ::kan-MX4 osh3Δ::LYS2 osh4Δ::HIS3 osh5Δ::LEU2 osh6Δ::LEU2 osh7Δ::HIS3* [*OSH4, TRP1*]	
CBY926	*SEY6210 osh1Δ::kan-MX4 osh2Δ::kan-MX4 osh3Δ::LYS2 osh4Δ::HIS3 osh5Δ::LEU2 osh6Δ::LEU2 osh7Δ::HIS3* [*osh4-1, TRP1*]	
CBY928	*SEY6210 osh1Δ::kan-MX4 osh2Δ::kan-MX4 osh3Δ::LYS2 osh4Δ::HIS3 osh5Δ::LEU2 osh6Δ::LEU2 osh7Δ::HIS3* [*osh4-2, TRP1*]	
CBY966	*CBY340 osh1Δ::kan-MX4 osh2Δ::kan-MX4 osh3Δ::LYS2 osh4Δ::HIS3 osh5Δ::LEU2 osh6Δ::LEU2 osh7Δ::HIS3* [*osh4-1, TRP1*] [*STE6*-HA, *URA3*]	
CBY968	*CBY340* [*STE6*-HA, *URA3*]	
CBY994	MATα *ura3Δ0 leu2Δ0 lys2Δ his3Δ1 arv1Δ::kan-MX4*	
CBY1024	MAT**a** *ura3Δ0 leu2Δ0 lys2Δ his3Δ1 las17Δ::kan-MX4* [*STE6*-HA, *URA3*]	
CBY1026	MAT**a** *ura3Δ0 met15Δ0 leu2Δ0 his3Δ::kan-MX4* [*STE6*-HA, *URA3*]	
DDY904	MATα *ura3-52 his3Δ200 lys2-801 leu2-3,112*	D. Drubin (University of California, Berkeley, USA)
DDY1438	*DDY904 las17Δ::URA3*	D. Drubin (University of California, Berkeley, USA)
JRY4130	MATα *ura3-52 his4-619 sec18*	
JRY6306	*CBY340 osh2Δ::URA3 osh4Δ::HIS3 osh5Δ::LEU2 osh6Δ::LEU2 osh7Δ::HIS3*	Beh et al., 2001
JRY6312	*SEY6210 osh1Δ::URA3 osh2Δ::URA3 osh4Δ::HIS3 osh5Δ::LEU2 osh7Δ::HIS3*	Beh et al., 2001
JRY6320	*CBY340 osh1Δ::URA3 osh2Δ::URA3 osh3Δ::LYS2 osh5Δ::LEU2 osh6Δ::LEU2 osh7Δ::HIS3*	Beh et al., 2001
JRY6326	*SEY6210 TRP1::*P^{MET3}*-OSH2 osh1Δ::kan-MX4 osh2Δ::kan-MX4 osh3Δ::LYS2 osh4Δ::HIS3 osh5Δ::LEU2 osh6Δ::LEU2 osh7Δ::HIS3*	Beh et al., 2001
RH286-1C	MAT**a** *ura3 his4 leu2 bar1 sla2/end4-1(ts)*	Raths et al., 1993
RSY255	MATα *ura3-52 leu2-3,112*	Novick and Schekman, 1979
RSY782	MATα *ura3-52 his4-619 sec1-1*	Novick and Schekman, 1979
SEY6210	MATα *ura3-52 his3Δ200 lys2-801 leu2-3,112 trp1Δ901 suc2Δ9*	Robinson et al., 1988
W303-1A	MAT**a** *ura3-1 his3-11 leu2-3,112 trp1-1 can1-100 ade2-1*	R. Rothstein (Columbia University, New York, USA)

*Unless otherwise stated, all strains were created as part of this study.

Ste6p internalization assay

Ste6p stability was analyzed as described previously (Wendland et al., 1999). Yeast transformed with a plasmid expressing HA-epitope-tagged Ste6p, pSM672 (Berkower et al., 1996), were grown to early log phase, harvested, and then resuspended to a density of 12.5 OD_{600} units ml^{-1} in 2.5 ml pre-warmed 37°C synthetic complete medium lacking uracil. The cultures were incubated for 1 hour at 37°C before the addition of 12.5 μl of 1 mg ml^{-1} cycloheximide. At the times indicated, 0.5 ml of each culture was removed and added to an equal volume of ice-cold 20 mM KF, 20 mM NaN_3, 50 μg ml^{-1} BSA. After centrifugation, each pellet was resuspended in 1 ml ice-cold distilled water and 150 μl of a 2 N NaOH, 80 μl ml^{-1} 2-mercaptoethanol solution and incubated on ice for 20 minutes. 150 μl 50% trichloroacetic acid was then added and the mixture was incubated on ice for an additional 30 minutes before centrifugation. After complete removal of supernatants, pellets were resuspended in 20 μl 0.5 M Tris-HCl pH 7.5 and 20 μl 2X sodium dodecyl sulfate (SDS) sample buffer, and incubated at 37°C for 30 minutes before loading on a 6% SDS polyacrylamide gel. After electrophoresis, resolved proteins were transferred to nitrocellulose (N-Hybond, Amersham, Arlington Heights, IL) and Ste6-HAp was detected using a mouse anti-HA antiserum (1:1000 dilution; Boehringer Mannheim, Indianapolis, IN) and a horseradish peroxidase (HRP)-conjugated goat anti-mouse secondary antiserum (1:3000 dilution). Ste6-HAp bands were visualized by chemiluminescence (ECL, Amersham, Arlington Heights, IL).

FM4-64 labeling

FM4-64 labeling was performed as previously described, but with minor modifications (Vida and Emr, 1995). FM4-64 internalization was examined in 5.0 OD_{600} units of cells harvested from cultures grown in synthetic medium at 23°C, resuspended in 500 μl of synthetic medium, and cultured for 30 minutes at 37°C. Cells were then treated with 32 μM FM4-64 for 30 seconds and immediately diluted with 10 ml of synthetic medium prewarmed at 37°C. After centrifugation, and a wash with warmed medium, cell pellets were resuspended in 0.5 ml of medium and incubated for an additional 30 minutes at 37°C before viewing by fluorescence microscopy. The use of FM4-64 to examine vacuolar morphology was performed as previously described (Kato and Wickner, 2001).

Exocytosis and CPY processing assays

Pulse-chase analyses of carboxypeptidase Y (CPY), Hsp150p and Gas1p transport were performed on 20 OD_{600} units of cells harvested from mid-log cultures grown in synthetic medium. For metabolic labeling, the cells were resuspended in 2.5 ml of synthetic medium prewarmed to 37°C and incubated at 37°C for 60 minutes before the addition of 250 μCi of Tran[^{35}S]-label (ICN Radiochemicals). After a 10 minute incubation, 25 μl of chase solution (200 mM $(NH_4)_2SO_4$, 2 mg ml^{-1} methionine, 2 mg ml^{-1} cysteine) was added and incubated at 37°C (for CPY maturation, a 5 minute incubation with Tran[^{35}S]-label was followed by the addition of chase solution). For each time

point, 0.5 ml of culture was removed and transferred to a microfuge tube on ice containing 50 μl of stop solution (100 mM NaN_3, 1 mg ml^{-1} cycloheximide). Cells and medium were separated by centrifugation.

For the analysis of Hsp150p secretion, radiolabeled glycoproteins secreted into the medium were precipitated using Concanavalin-A (Con-A) Sepharose as described (Holthuis et al., 1998). Cells were disrupted with glass beads and intracellular glycoproteins were precipitated from the cleared lysate after binding to Con-A Sepharose. Secreted glycoproteins, of which Hsp150p is the most abundant (Russo et al., 1992; Gaynor and Emr, 1997), were visualized by autoradiography following SDS-PAGE and fluorography.

CPY and Gas1p were immunoprecipitated from the cleared lysate of cell extracts using specific antibodies (both antibodies were gifts from the Schekman lab, University of California, Berkeley, CA) and protein A-Sepharose as previously described (Rose et al., 1989). Radiolabeled immunoprecipitates were analyzed by SDS polyacrylamide electrophoresis and visualized following fluorography.

CPY mis-sorting assay

Extracellular secretion of CPY from yeast grown on solid synthetic medium was analyzed as previously described (Roberts et al., 1991) with a few modifications. Cells were streaked in patches onto solid synthetic medium that lacks methionine, grown overnight at 30°C, and then transferred by replica printing onto solid media containing varying methionine concentrations. The methionine concentrations used repressed expression of *OSH2* in the *osh*Δ P^{MET3}-*OSH2* strain (JRY6326) to varying degrees as manifested in growth-rate differences. After another night of growth at 30°C, nitrocellulose filters were placed on top of the patched cells in direct contact with the solid medium, and incubated for 12 hours at 30°C. Once removed from the solid medium, the nitrocellulose filters were washed several times with Buffer A (20 mM Tris-HCl pH 7.6, 150 mM NaCl, 2% dry milk) to dislodge bound cells. The filters were probed with the rabbit polyclonal anti-CPY antiserum in Buffer A (1:2000 dilution), washed with Buffer A, and then incubated with a HRP-conjugated goat anti-rabbit secondary antiserum (1:5000 dilution; Amersham) in Buffer A.

Transmission electron microscopy

Cells were prepared for electron microscopy as described (Wright, 2000). Cells were fixed overnight at 4°C in 0.5% glutaraldehyde followed by a 45 minute postfixation at room temperature with 2% $KMnO_4$ (low mercury; Aldrich Chemical, Milwaukee, WI). Samples were en bloc stained with 1% uranyl acetate, dehydrated with absolute ethanol, infiltrated and embedded in Spurr's resin (Electron Microscopy Sciences, Ft Washington, PA). Thin sections were stained with uranyl acetate and Reynold's lead citrate. Sections were viewed at 100 kV on a FEI Tecnai 12 transmission electron microscope.

Results

Depletion of Osh proteins disrupted vacuolar morphology and caused lipid droplet accumulation

Deletion of all seven yeast *OSH* genes causes lethality. This inviability can be rescued by expression of any of the individual *OSH* genes indicating that the *OSH* genes share at least one essential overlapping function (Beh et al., 2001). To define the essential functions mediated by the *OSH* family, we investigated the cellular defects associated with the elimination of all *OSH* function. We created two independent strains in which six *OSH* genes were deleted and the seventh was replaced with a construct permitting exogenous control of its expression. In one strain, *OSH* function was gradually depleted by repressing the synthesis of the sole remaining *OSH* gene, *Osh2*. In the other strain, the single remaining *OSH* gene, *Osh4*, contained a temperature-sensitive mutation and could be rapidly inactivated when cultured at higher temperatures. The effects of inactivating all the *OSH*s were then observed in both strains.

The first strain examined lacked six of the seven *OSH* genes, and the remaining *OSH2* gene was regulated by the *MET3* promoter (JRY6326) (Beh et al., 2001). In the presence of added methionine, *OSH2* expression was repressed and the *osh*Δ P^{MET3}-*OSH2* strain ceased to grow (*osh*Δ refers to the deletion of all *OSH* genes other than those indicated). Growth arrest was gradual, taking about four culture doublings. The second yeast strain analyzed also lacked all chromosomal copies of the *OSH* genes but was viable because it carried a plasmid with one of two *KES1*/*OSH4* temperature-sensitive mutations, *osh4-1(ts)* and *osh4-2(ts)*. At 37°C, the mutant proteins encoded by these *OSH4* alleles were inactivated and the *osh*Δ *osh4(ts)* strains stopped growing. After the shift to the restrictive temperature, growth was retarded within 15 minutes and completely arrested within an hour. After culturing *osh*Δ *osh4(ts)* cells under these conditions, their inviability could be reversed by returning the cells to the lower permissive temperature for growth. When *osh*Δ *osh4(ts)* cells were incubated at 37°C for 1 hour and then micromanipulated onto solid medium and grown at 23°C, 88% (14 out of 16) recovered and formed colonies (92% of wild-type and 96% *osh*Δ *OSH4* cells recovered after the same treatment). Using these strain constructions we monitored specific changes in cellular morphology that resulted from rapid inactivation of *OSH4*, or gradual depletion of Osh2p, in cells that otherwise lacked all *OSH* family genes.

After *OSH2* expression was repressed, the *osh*Δ P^{MET3}-*OSH2* cells exhibited drastic morphological changes. The effect of eliminating all *OSH* genes was analyzed by transmission electron microscopy using fixation methods designed to accentuate membranous structures (Fig. 1). We observed defects consistent with abnormal cell wall deposition (Fig. 1B). Along the perimeter of the cell surface the thickness of the cell wall varied, whereas in wild-type cells it was uniform. The abnormal depositions seen by electron microscopy were probably irregular deposits of chitin (other than bud scars). In Osh-depleted cells stained with calcofluor and examined by fluorescence microscopy, chitin was often mislocalized at the bud tip in budding daughter cells and randomly dispersed over the cell surface (Fig. 2). Defects in cell size and budding were also apparent. Many of the arrested cells were significantly larger than wild type. Septation of dividing cells was often incomplete, and cells with multiple buds were observed with buds oriented randomly with respect to one another, indicating a budding pattern defect. The gradual depletion of Osh proteins also caused observable changes within the cell. Many cells accumulated vesicles and the number of cytoplasmic lipid droplets increased (Fig. 1B). In nearly all cells, significant vacuolar fragmentation and collapse was observed, and within these vacuolar remnants numerous small lipid droplets were evident. The defects associated with the gradual depletion of Osh proteins indicated that the *OSH*s were important for processes both at the cell surface and within the cell itself.

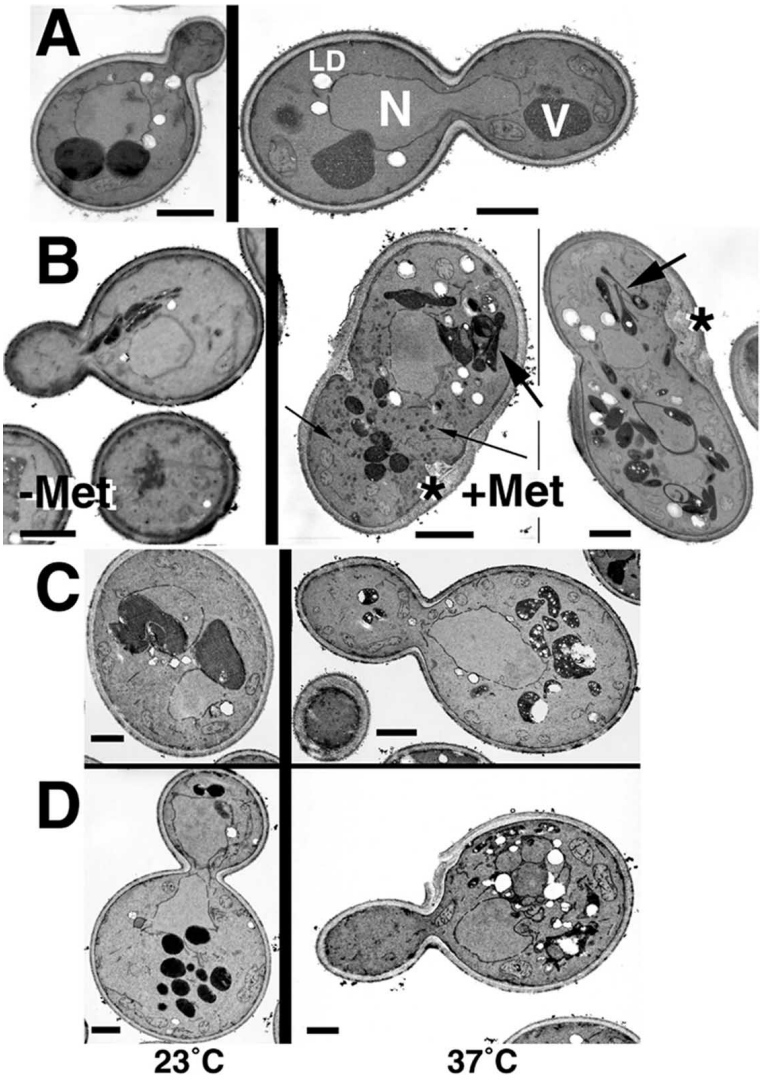

Fig. 1. Electron micrographs of Osh protein-depleted cells and *OSH* temperature-sensitive mutants. (A) Wild-type, (B) *osh*Δ P^{MET3}-*OSH2*, and (C and D) *osh*Δ *osh4(ts)* cells, were examined by electron microscopy. V, vacuole; N, nucleus; LD, lipid droplets. Thick arrows indicate the large dark irregular structures that correspond to fragmented and collapsed vacuoles, thin arrows indicate vesicles, asterisks indicate cell wall abnormalities. (A) Wild-type cells (SEY6210) contained an average of 2.5 lipid droplets (s.d.=2.1; 54 random sections counted); only 2% of wild-type cells (1/54) accumulated more than twenty-five 50 nm vesicles; 2% of wild-type cells (1/54) had pronounced cell wall defects; 2% exhibited vacuolar fragmentation (1/54); and in only 10% of sections with vacuoles (5/50) were <100 nm vacuolar droplets observed. (B) In the absence of methionine (–Met), *OSH2* was expressed in *osh*Δ P^{MET3}-*OSH2* cells (JRY6326), which were viable, but compared with wild-type cells defects were nonetheless observed. In random sections, an average of 2.6 lipid droplets were counted (s.d.=2.5; 70 sections counted); 6% of growing *osh*Δ P^{MET3}-*OSH2* cells (4/63) exhibited cell wall defects; 5% had an accumulation of more than 25 50 nm vesicles (4/75); 39% exhibited vacuolar fragmentation (25/64); and in 61% of vacuole-containing sections (37/61), small <100 nm vacuolar lipid droplets were observed. After methionine addition (+Met) and the gradual depletion of Osh proteins in *osh*Δ P^{MET3}-*OSH2* cells, the average number of lipid droplets was 8.1 (s.d.=6.7; 30 sections counted); 47% of Osh-depleted cells (14/30) had pronounced cell wall defects; in 30% of random sections (9/30) more than twenty-five 50 nm vesicles accumulated; 80% of random sections (24/30) contained aberrant, dark-staining vacuolar remnants; and in 81% of sections with vacuoles (26/32), <100 nm vacuolar lipid droplets were observed. (C) *osh*Δ *osh4-1* cells, and (D) *osh*Δ *osh4-2* cells were cultured either at 23°C or at 23°C and then for 1 hour at 37°C. For *osh*Δ *osh4-2* cells at 23°C, an average of 3.5 lipid droplets were observed (s.d.=3.4; 41 sections counted); 37% exhibited vacuolar fragmentation (18/49); 9% accumulated more than twenty-five 50 nm vesicles (4/46); and 10% had pronounced cell wall defects (6/62). At 37°C, *osh*Δ *osh4-2* cells contained an average of 4.4 lipid droplets (s.d.=4.8; 52 sections counted); 62% exhibited vacuolar fragmentation (29/47); 10% accumulated more than twenty-five 50 nm vesicles (6/61); and 15% had pronounced cell wall defects (10/65). Bars, 1 μm.

Many, but not all, of the defects observed after gradual Osh depletion were seen when *OSH* function was inactivated more rapidly. One hour after the shift to the restrictive temperature of growth the *osh*Δ *osh4(ts)* cells were still wild type in size, and no cell wall abnormalities were apparent (Fig. 1C,D). Within these cells, however, cytoplasmic lipid droplets accumulated and extensive vacuolar fragmentation was seen. As previously observed after the gradual depletion of Osh2p, vacuolar remnants were often filled with small lipid droplets in *osh*Δ *osh4(ts)* cells. Thus, regardless of the strain, vacuolar morphology and lipid droplet distribution were disrupted in cells depleted of *OSH* function. At the permissive temperature, *osh*Δ *osh4(ts)* strains grew more slowly than wild type and exhibited many of the same defects (although less severe) as those observed after growth arrest at 37°C. Thus, regardless of how *OSH* function was eliminated, loss of *OSH* function resulted in vacuolar fragmentation and lipid droplet accumulation.

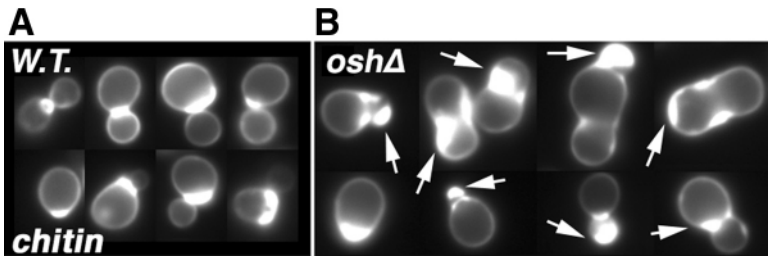

Fig. 2. Osh protein depletion caused defective chitin accumulation. Calcofluor staining of yeast cells viewed by fluorescence microscopy shows chitin deposition. (A) Chitin bud scars are visible in wild-type cells (SEY6210) at the mother-bud junction or immediately adjacent, which reflects the axial pattern of haploid budding. (B) In *osh*Δ P^{MET3}-*OSH2* cells (JRY6326) after methionine repression of *OSH2* expression, Osh depletion caused chitin to accumulate at abnormal sites other than just the mother-bud junction (e.g. bud tip). Arrows indicate abnormal deposits of chitin. Exposure times for *osh*Δ P^{MET3}-*OSH2* cells were shorter that wild type indicating a comparatively greater amount of chitin.

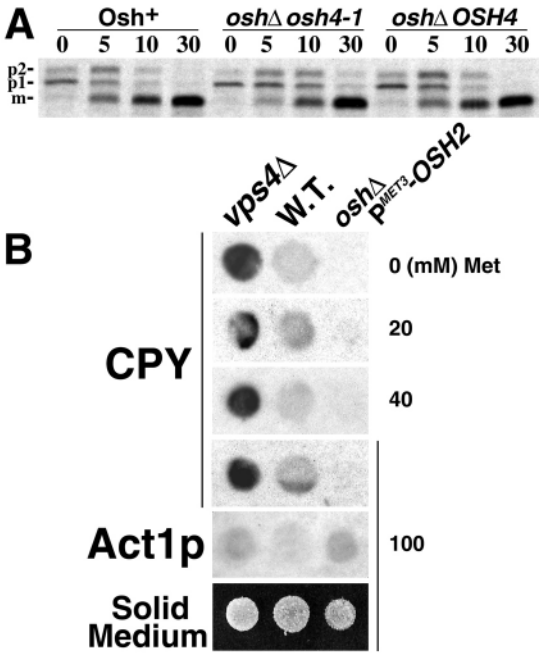

Fig. 3. CPY maturation and sorting was unaffected by loss of all *OSH* function. (A) Autoradiograph of CPY immunoprecipitations from wild-type (Osh$^+$; SEY6210), *osh*Δ *osh4-1* (CBY886) and *osh*Δ *OSH4* (JRY6320) cultures. p1, ER/early Golgi form of CPY; p2, late Golgi CPY; m, mature vacuolar form of CPY. Cells were pulse-labeled with Tran[^{35}S]-label for 5 minutes and chased for the periods indicated at 37°C. CPY was immunoprecipitated from cell lysates and analyzed by SDS-PAGE. (B) CPY immunoblots of *vps4*Δ (CBY824), wild-type (W.T.; SEY6210), and *osh*Δ P^{MET3}-*OSH2* (JRY6326) strains. Strains were spotted on solid media with increasing concentrations of methionine (up to 100 mM), which repressed expression of *OSH2* in the *osh*Δ P^{MET3}-*OSH2* strain and arrested growth. Filters were placed directly on the solid medium and CPY secreted from cells was detected with anti-CPY antibodies (Roberts et al., 1991). Filters were also probed with anti-Act1p to detect the discharge of actin from non-specific cell lysis. Equivalent amounts of cells were spotted on the solid medium as shown by the example in the bottom panel.

Exocytosis and transport of carboxypeptidase Y (CPY) to the vacuole were unaffected by Osh depletion

The elimination of all *OSH* function caused aberrant vacuolar morphology, and in some cases vesicle accumulation, suggesting that secretory transport to the vacuole or to the cell surface might be disrupted. Moreover, several reports suggest that OSBP homologs regulate vesicular trafficking through the Golgi (Fang et al., 1996; Xu et al., 2001). To test whether *OSH* genes affected vesicular trafficking of proteins from the ER to the vacuole, the maturation of CPY precursors in *OSH* mutants was analyzed. In wild-type cells, the p1 precursor form of CPY is generated when newly synthesized CPY is translocated into the ER and then core glycosylated. After transport from the ER to the Golgi, CPY is further glycosylated to the larger p2 precursor form. Finally, upon arrival in the vacuole, the smaller mature (m) CPY protein is produced through proteolytic removal of the pro-CPY leader peptide. To inactivate *OSH* function before pulse-chase labeling, the *osh*Δ *osh4-1*(*ts*) strain (and the other control strains examined) were incubated for 60 minutes at 37°C. After pulse-chase labeling, CPY was immunoprecipitated from extracts of wild-type and the *OSH* mutant strains. CPY processing showed similar kinetics in all the strains tested (Fig. 3*A*) indicating that CPY maturation was similar to wild-type in *osh*Δ *osh4-1* and *osh*Δ *OSH4* mutant strains. The only apparent difference was a slight delay in the conversion of the p1 precursor into the p2 form in the *osh*Δ *osh4-1* strain, when compared with the *osh*Δ *OSH4* or wild-type strains. In fact, a similar subtle lag in CPY processing has been reported in other mutants that affect sterols, including viable *ERG* mutants (Munn et al., 1999). These results indicated that the *OSH* genes do not significantly affect CPY transport from the ER to the Golgi, or from the Golgi to the vacuole.

Some secretory mutants do not affect CPY delivery to the vacuole, but rather secrete a large proportion of CPY out of the cell. In these mutants, the p2 form of CPY is mis-sorted to the plasma membrane and some is released into the medium (reviewed by Bryant and Stevens, 1998). To evaluate whether any CPY was secreted from the cell after *OSH* gene inactivation, we took advantage of the gradual growth arrest caused when *OSH2* expression was repressed in the *osh*Δ P^{MET3}-*OSH2* strain. Patches of *osh*Δ P^{MET3}-*OSH2* cells were transferred onto solid medium containing a range of methionine concentrations. In the presence of added methionine, expression of the integrated P^{MET3}-*OSH2* construct was repressed and growth of this strain slowed, especially at higher methionine concentrations. Extracellular secretion of CPY was monitored by overlaying nitrocellulose filters directly onto patches of yeast strains grown on solid media (Fig. 3B). Using anti-CPY antibodies, the filters were probed for the presence of secreted CPY. As a control, duplicate filters were probed with antiserum that recognizes actin. Although polymerized actin comprises the basic structure of the cytoskeleton, lower levels of monomeric actin are present in the cell (Karpova et al., 1998) and can be nonspecifically released by cell lysis with other cytoplasmic proteins. The nitrocellulose immunoblots were taken from comparable patches of cells grown on solid medium (bottom panel of Fig. 3B*)*. As a control, CPY extracellular secretion was also monitored in a *vps4*Δ strain. *VPS4* is required for the sorting and trafficking of CPY from the *trans*-Golgi to the vacuole (Robinson et al., 1988; Rothman et al., 1989). The *vps4*Δ strain secreted a large amount of CPY onto nitrocellulose, but relative to wild type the *vps4*Δ mutant did not release actin indicating specific CPY release (Fig. 3B). In comparison, the *osh*Δ P^{MET3}-*OSH2* strain did not release actin or CPY, regardless of the extent of *OSH2* repression. Based on these experiments, reducing *OSH* function had no adverse effect on CPY sorting at the *trans*-Golgi.

The exocytosis of several other secreted proteins were also unaffected by *OSH* inactivation. To determine whether secretion to the plasma membrane was affected by *OSH* mutants, transport of the glycoprotein Hsp150p and the glycosyl-phosphatidylinositol (GPI)-anchored protein Gas1p were examined following pulse-chase radiolabeling (Fig. 4). Hsp150p is the most abundant glycoprotein secreted into the medium (Russo et al., 1992; Gaynor and Emr, 1997), and Gas1p is transported to the plasma membrane where it is associated with membrane regions rich in ergosterol (Bagnat et al., 2000). To examine Hsp150p secretion, glycoproteins

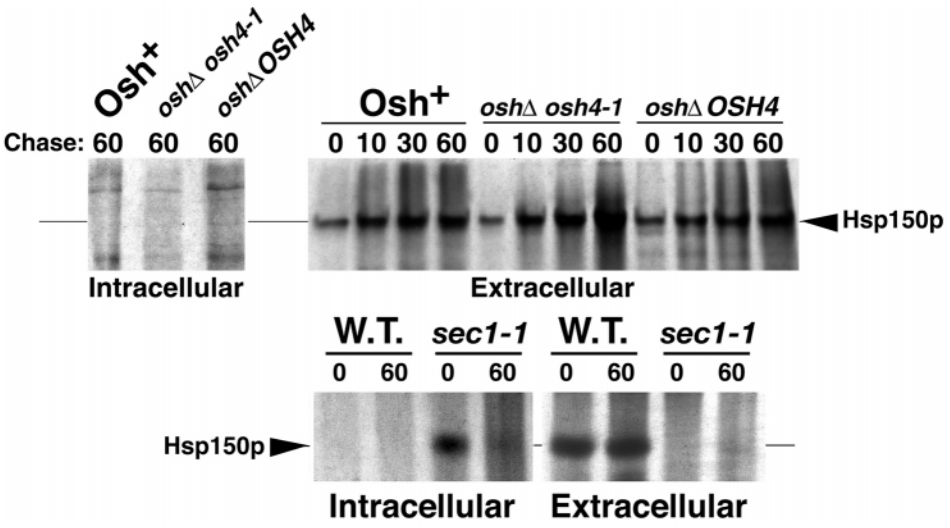

Fig. 4. Secretion of Hsp150p to the cell surface was unaffected by *OSH* temperature-sensitive mutants. Autoradiograph of Hsp150 purified using Con A-affinity chromatography from the extracellular medium and cell extracts of wild-type (Osh$^+$; SEY6210), *osh*Δ *osh4-1* (CBY926), *osh*Δ *OSH4* (CBY924), wild-type (W.T.; RSY255) and *sec1-1* (RSY782) strains. Cultures were incubated at 37°C for 60 minutes and, after a 10 minute pulse with [^{35}S]-label followed by the addition of the chase solution, samples were removed at 0, 10, 30 and 60 minutes. In all samples from *OSH* mutants, Hsp150p was secreted into the medium with equivalent kinetics to its wild-type control. Moreover, 60 minutes after pulse labeling and addition of chase solution no intracellular Hsp150p was detectable. In the exocytosis-defective *sec1-1* strain scarcely any Hsp150p was secreted into the medium during the 60 minutes following pulse labeling and addition of chase solution, and Hsp150p was detected within cells (internalized Hsp150p appeared to degrade 60 minutes after the addition of chase solution but was nonetheless detectable). The autoradiograph of intracellular glycoproteins represented a longer exposure than that showing secreted extracellular glycoproteins.

were purified from the extracellular medium and from solubilized cell extracts after a 60 minute incubation at 37°C, and pulse/chase labeled as described in the Materials and Methods. In wild-type, *osh*Δ *OSH4* and *osh*Δ *osh4-1* strains, Hsp150p was secreted into the medium with equal kinetics and there was no detectable intracellular accumulation (Fig. 4). By contrast, in a *sec1-1* mutant, which is defective for the transport of secretory proteins from the Golgi to the plasma membrane, Hsp150p was not secreted into the medium but remained within the cell (Fig. 4).

Gas1p transport to the plasma membrane was also unaffected by *OSH* inactivation. After a 60 minute incubation at 37°C and a 10 minute pulse/chase labeling, the conversion of the 105 kDa Gas1p precursor to the plasma membrane-associated 125 kDa mature form was similar in wild-type, *osh*Δ *OSH4* and *osh*Δ *osh4-1* strains (Fig. 5). In contrast, mature Gas1p was not observed in the *sec18(ts)* mutant, which is defective in exocytosis at 37°C. These results indicate that Gas1p transport to the plasma membrane was not defective in the *OSH* mutants. In similar pulse/chase experiments, invertase secretion to the plasma membrane was also unaffected in *osh*Δ *osh4-1* cells (C.T.B., unpublished data).

OSH mutants disrupted the internalization step of endocytosis

We tested whether endocytosis, another major trafficking pathway, was affected by the elimination of *OSH* gene function. As demonstrated by several independent assays, Osh depletion had a significant effect on endocytosis from the cell surface into the cell. In the first endocytosis assay, the internalization of a marker dye for fluid-phase endocytosis, lucifer yellow, was measured by fluorescence microscopy (Fig. 6). In almost all wild-type cells grown at either 23°C or 37°C, lucifer yellow was efficiently internalized from the medium and accumulated in the vacuole. By contrast, lucifer yellow uptake was blocked in *osh*Δ *osh4(ts)* cells after a 60 minute incubation at the restrictive temperature (Fig. 6). In the majority of *osh*Δ *osh4(ts)* cells, internal lucifer yellow staining was reduced and only in a few cells was the fluorescence in vacuolar fragments equal in intensity to wild-type vacuoles. The percentage of faintly stained Osh-depleted cells (~85%) was similar to the well-characterized endocytosis mutant, *las17*Δ (87%), indicating a comparable defect. *LAS17/BEE1* encodes the *Saccharomyces cerevisiae* homolog of the mammalian Wiskott-Aldrich syndrome protein, which is required for cortical actin assembly and endocytosis (Li, 1997; Naqvi et al., 1998). Although some endocytosis genes are essential, *LAS17* is only required for growth at high temperatures. Lesser defects in lucifer yellow uptake were detected in both *osh*Δ *OSH4* cells grown at 23°C or 37°C, and also in *osh1*Δ *osh4(ts)* cells grown at the permissive temperature of 23°C. These findings indicated that *OSH* genes are required for fluid-phase endocytosis.

To determine whether Osh depletion affected other aspects of endocytosis, we analyzed the endocytic internalization and subsequent proteolysis of Ste6p, a plasma membrane protein required for export of **a**-factor mating pheromone (Kuchler

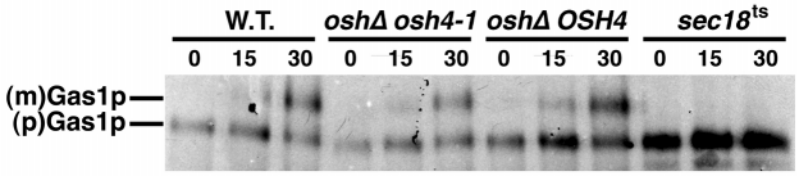

Fig. 5. Secretion of Gas1p to the plasma membrane was unaffected by *OSH* mutants. Autoradiograph of Gas1p immunoprecipitations from wild-type (W.T.; SEY6210), *osh*Δ *osh4-1* (CBY886), *osh*Δ *OSH4* (JRY6320) and *sec18(ts)* (JRY4130) cell lysates following SDS-PAGE. (p)Gas1p, precursor form of Gas1p; (m)Gas1p, mature plasma membrane form of Gas1p. After an incubation of 1 hour at 37°C, cells were pulse-labeled for 5 minutes and chased for the periods indicated (in minutes) at 37°C.

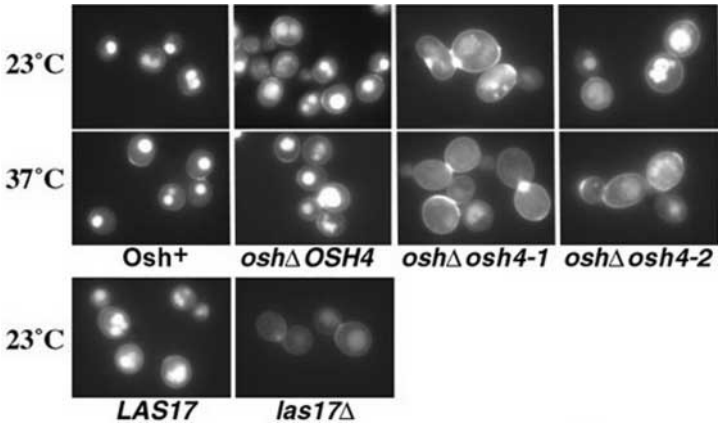

Fig. 6. Temperature-sensitive *OSH* mutants were defective for lucifer yellow fluid-phase endocytosis. Lucifer yellow uptake and delivery to the vacuole was observed at 23°C, or after a 60 minute incubation at 37°C, in wild-type (Osh$^+$; SEY6210), *osh*Δ *OSH4* (JRY6320), *osh*Δ *osh4-1* (CBY886) and *osh*Δ *osh4-2* (CBY892) cells. For comparison, lucifer yellow uptake was examined at 23°C in wild-type *LAS17* (DDY904) and *las17*Δ (DDY1438) cells. In the wild-type Osh$^+$ strain, vacuoles that were brightly stained with lucifer yellow were observed in 92% of cells grown at 23°C (65 out of 71 cells counted) and an equivalent percentage was seen at 37°C (91%; 64/70). In *osh*Δ *OSH4* cells, 68% exhibited brightly staining vacuoles at 23°C (69/101) and an equivalent percentage was observed at 37°C (69%; 69/99). In *osh*Δ *osh4-1* cells at 23°C, however, 42% exhibited bright lucifer yellow staining (36/85), and at 37°C, only 13% of cells (10/75) efficiently internalized lucifer yellow. Likewise, at 23°C 44% of *osh*Δ *osh4-2* cells (34/78) had bright fluorescent vacuoles and vacuolar remnants, and at 37°C, only 17% of these cells (13/79) were brightly stained. This result was comparable to that observed in the endocytosis mutant *las17*Δ. Only 13% of *las17*Δ cells (15/116) were as brightly stained as in the wild-type parent, where 93% of the wild-type *LAS17* cells (78/84) had efficiently absorbed lucifer yellow from the medium. All photographs represent equal exposures.

et al., 1989). In wild-type cells, Ste6p is constitutively internalized from the plasma membrane and routed to the vacuole where it is degraded (Berkower et al., 1994). The stability of Ste6p is markedly increased in endocytosis mutants, which effectively block the delivery of Ste6p to vacuolar proteases. The stability of epitope-tagged Ste6p-HA was analyzed in the *osh*Δ *osh4-1* temperature-sensitive mutant, the *las17*Δ endocytosis mutant, and their respective wild-type control strains (Fig. 7A). After 60 minutes at 37°C, nearly all Ste6p-HA was degraded in the wild-type strains, but significant levels of Ste6p-HA persisted in both the *osh*Δ *osh4-1* and *las17*Δ mutants (Fig. 7A). Even after 90 minutes, Ste6p-HA was detectable in the *osh*Δ *osh4-1* and *las17*Δ samples. These findings indicated a comparable disruption of Ste6p-HA internalization in *osh*Δ *osh4-1* and *las17*Δ mutants. Moreover, the defect in Ste6p degradation was not due to a failure in vacuolar proteolysis because the proteolytic processing of CPY was unaffected in *osh*Δ *osh4-1* cells (see above).

OSH mutant cells were also defective in the endocytic internalization of the fluorescent lipophilic dye, FM4-64. FM4-64 associates with the yeast plasma membrane and, following endocytosis, it is delivered to the vacuole where it stains the vacuolar membrane (Vida and Emr, 1995). In wild-type cells, FM4-64 was internalized and concentrated in the vacuole (Fig. 7B). In *osh*Δ *OSH4* and *osh*Δ *osh4-1* cells, FM4-64 fluorescence was less intense indicating a reduction in dye internalization. Despite comparable defects in lucifer yellow uptake, the FM4-64 endocytosis defect in *las17*Δ mutants was more pronounced than in *osh*Δ *osh4-1* cells (see Fig. 10B for comparison) suggesting that *LAS17* and the *OSH* genes affect endocytosis in a different manner. Taken together, the results of all endocytosis assays established that an important function of the *OSH*s is related to endocytosis.

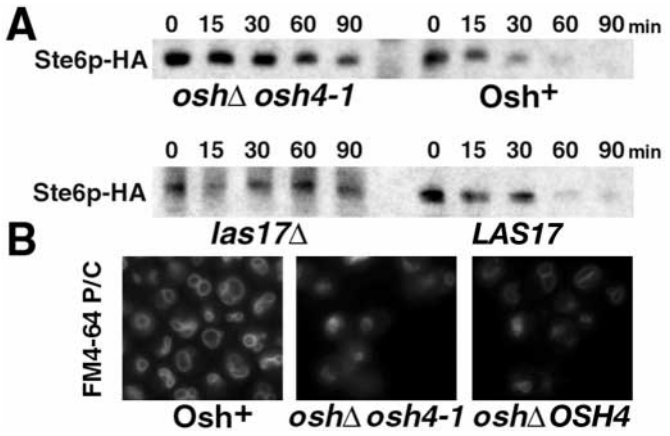

Fig. 7. FM4-64 uptake, and Ste6p internalization and degradation, were inhibited in an *OSH* temperature-sensitive mutant. (A) Protein immunoblots of hemagglutinin (HA) epitope-tagged Ste6p expressed in *osh*Δ *osh4-1* cells (CBY966) and its congenic wild-type Osh$^+$ parent (CBY968), and *las17*Δ cells (CBY1024) and its congenic wild-type *LAS17* parent (CBY1026). In each of these strains, the stability of Ste6p was analyzed by adding cycloheximide to stop protein synthesis and then removing, at the times indicated, equal volumes of cell culture incubated at 37°C. Extracted proteins were separated on SDS gels and analyzed by immunoblot with antibodies that recognized the HA epitope. Note that in the wild-type strains, Ste6p-HA degradation occurred after 60 minutes but in the *OSH* temperature-sensitive mutant and *las17*Δ strain Ste6p-HA persisted beyond 90 minutes. All strains were incubated for 1 hour at 37°C before the addition of cycloheximide. (B) Wild-type cells (Osh$^+$; SEY6210), *osh*Δ *osh4-1* (CBY926) and *osh*Δ *OSH4* (CBY924) cells were incubated for 30 minutes at 37°C, then treated with a short pulse of FM4-64 and chased with fresh medium. Cells were viewed by fluorescence microscopy 30 minutes after the FM4-64 pulse/chase (P/C) and photographs were taken with equal exposures.

OSH mutants affected sterol lipid distribution

In Osh-depleted cells, ergosterol levels increase 3.5-fold relative to wild type (Beh et al., 2001). This result suggests that ergosterol levels might be elevated at the plasma membrane, the normal cellular destination of unesterified ergosterol. However, many viable *OSH* deletion mutants are resistant to the ergosterol-binding antibiotic nystatin (Jiang et al., 1994; Beh et al., 2001) even though many nystatin-resistant strains have *reduced* levels of ergosterol exposed on the cell surface (Woods, 1971; Walker-Caprioglio et al., 1989). To resolve this

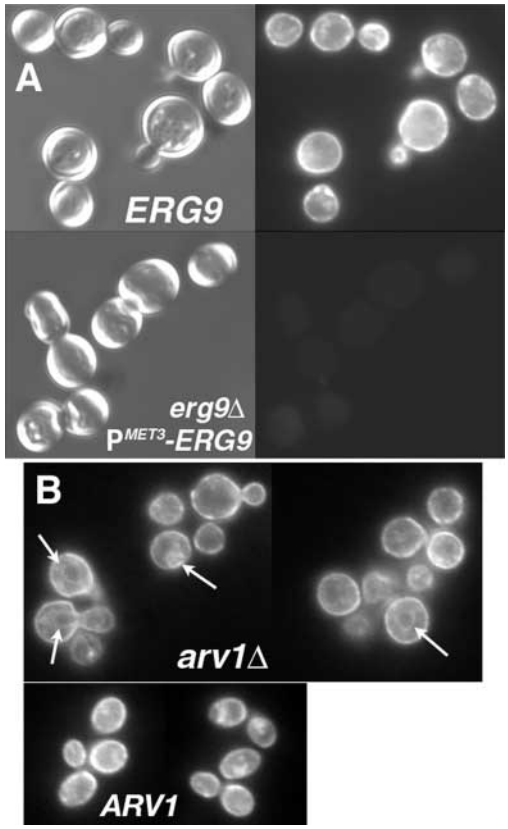

Fig. 8. Filipin specifically stained yeast sterols. (A) Wild-type *ERG9* (CBY858) and *erg9*Δ P^{MET3}-*ERG9* (CBY745) cells were treated with filipin. The left panels show cell morphology by DIC, and the right panels show the corresponding filipin staining observed by fluorescence microscopy. After addition of methionine, filipin fluorescence in *erg9*Δ P^{MET3}-*ERG9* cells was considerably less intense than in wild-type *ERG9* cells. Photographs were taken with equivalent exposures, although with longer exposures background filipin fluorescence was detectable in the *ERG9*-repressed cells. (B) Sterol distribution in both *arv1*Δ (CBY994) and wild-type *ARV1* (CBY858) cells were also examined using filipin fluorescence. In 41% of *arv1*Δ cells (52 out of 136 cells), fluorescence was observed within the cells whereas in wild-type cells, only 10% of cells (10/96) exhibited a comparable staining pattern. Arrows indicate filipin fluorescence associated with internal membranes.

apparent paradox, we analyzed in vivo the intracellular distribution of sterol lipids in *OSH* mutant cells.

In mammalian cells, the distribution of free cholesterol can be visualized by fluorescence microscopy using the cholesterol probe, filipin (Severs, 1997). Although filipin binds cholesterol with greater affinity than ergosterol (Brittman et al., 1974), filipin fluorescence was successfully adapted for analyzing yeast sterol-lipid distribution. Filipin/sterol fluorescence was observed primarily at the cell surface (Fig. 8A), where the bulk of free ergosterol is located in yeast. Fluorescence was also observed in small cytoplasmic spots, which might correspond to ergosterol-rich endocytic vesicles. Limited overlap between the filipin fluorescent spots and Nile Red stained lipid droplets was observed indicating that some, but not all filipin-fluorescent spots, corresponded to lipid droplets (C.T.B., unpublished data).

To evaluate the specificity of filipin/sterol staining in yeast, filipin fluorescence was examined in cells after sterol synthesis was blocked. *ERG9* is an essential gene that encodes squalene synthase, the first enzyme in the ergosterol biosynthetic pathway that is specific for sterol-lipid synthesis. A strain was created in which the wild-type *ERG9* gene was replaced with an integrated P^{MET3}-*ERG9* construct. In the presence of methionine, expression of squalene synthase was repressed and the P^{MET3}-*ERG9 erg9*Δ cells did not grow. Compared with filipin-stained wild-type cells, filipin fluorescence was diminished in growth-arrested P^{MET3}-*ERG9 erg9*Δ cells (Fig. 8A). This result indicated that filipin was a specific probe for yeast sterols because filipin fluorescence was significantly reduced in yeast compromised for sterol synthesis.

To determine whether filipin fluorescence could be used to detect aberrant sterol distribution, an *arv1*Δ mutant was treated with filipin. *ARV1* encodes a predicted zinc-binding integral membrane protein involved in the maintenance of normal ergosterol distribution in yeast cells (Tinkelenberg et al., 2000). In *arv1*Δ and wild-type cells, most ergosterol is present at the plasma membrane. However, in *arv1*Δ cells some ergosterol can be found in fractions corresponding to the endoplasmic reticulum (ER) and the vacuole (Tinkelenberg et al., 2000), organelles that are normally sterol deficient (Zinser et al., 1991). In *arv1*Δ cells filipin fluorescence was always observed at the cell periphery but in some cells fluorescence was also observed within the cell (Fig. 8B), which was rarely observed in wild-type cells. These results demonstrated that filipin fluorescence could be used in yeast to detect even subtle changes in intracellular sterol distribution.

Our previous analysis of all *OSH* deletion combinations identified two viable strains that were particularly resistant to nystatin (Beh et al., 2001). To examine sterol distribution in these strains, *osh*Δ *OSH1 OSH3* and *osh*Δ *OSH3 OSH6*, cells were treated with filipin and viewed by fluorescence microscopy (Fig. 9A). The staining patterns observed in these *OSH* mutants differed from that in wild type. Overall, fluorescence was greater in the *OSH* mutants than in wild-type cells. Within these cells, sterol distribution was most affected in the *osh*Δ *OSH3 OSH6* mutant, where a majority of cells exhibited aberrantly intense cytoplasmic filipin fluorescence. Unlike *arv1*Δ cells, the internal staining was characterized by bright staining spots and sinuous strands. Moreover, compared with wild type, a reduced number of *osh*Δ *OSH3 OSH6* cells were observed with intense plasma membrane staining. Only a subtle increase in cytoplasmic fluorescence was observed in *osh*Δ *OSH1 OSH3* cells and, between wild-type and *osh*Δ *OSH1 OSH3* cells, there was no discernible difference in plasma membrane fluorescence. In this context, nystatin resistance appeared to be a more sensitive measure of ergosterol defects at the plasma membrane than filipin staining. These findings indicated that in at least one *OSH* mutant strain the maintenance of normal sterol levels in the plasma membrane was defective and that sterols accumulated in internal membranes.

To determine whether sterol distribution was affected by loss of all the Osh proteins, *osh*Δ P^{MET3}-*OSH2* cells, and *OSH* temperature-sensitive *osh*Δ *osh4-1* and *osh*Δ *osh4-2* cells were examined by microscopy after filipin treatment (Fig. 9B,C). When *OSH2* was expressed, *osh*Δ P^{MET3}-*OSH2* cell morphology and filipin/sterol staining were comparable to wild-type cells although some internal filipin fluorescence was

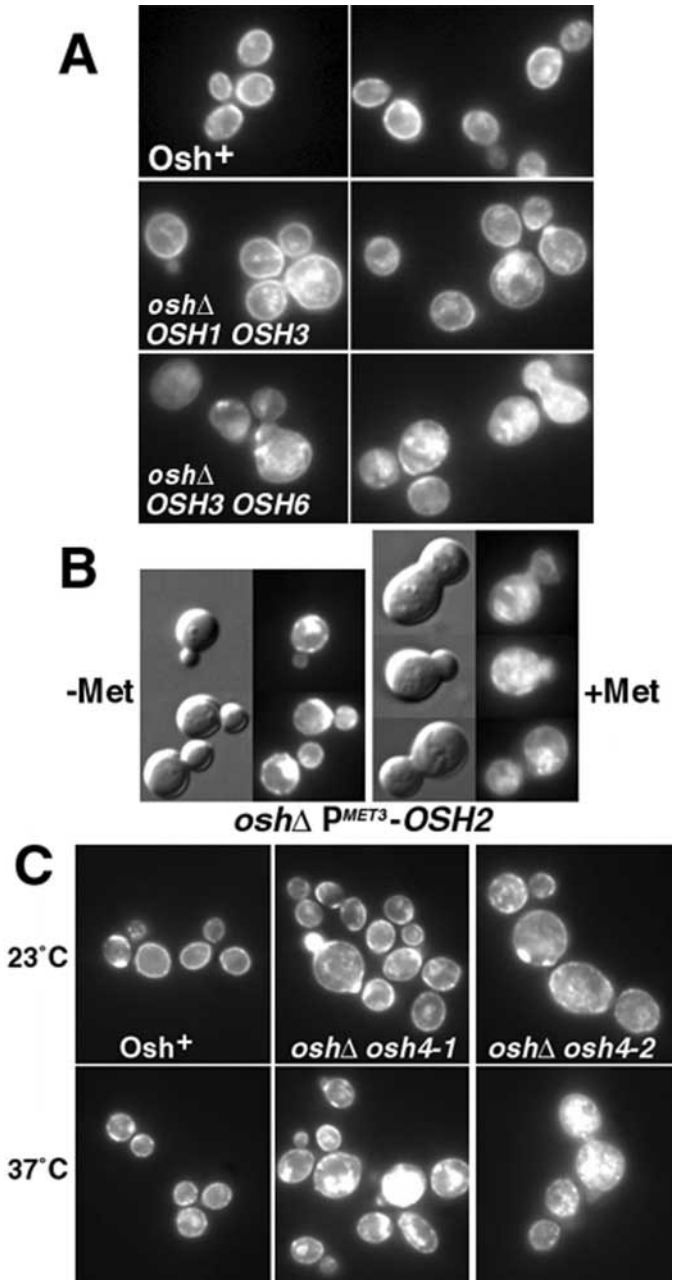

Fig. 9. Sterol lipid distribution was disrupted in *OSH* mutants. (A) The pattern of filipin fluorescence observed in wild-type cells (Osh$^+$; SEY6210) was disrupted in *osh*Δ *OSH1 OSH3* (JRY6306) and *osh*Δ *OSH3 OSH6* (JRY6312) mutant cells. Bright fluorescence at the plasma membrane was observed in 98% of wild-type cells (54 out of 55 cells counted), 98% of *osh*Δ *OSH1 OSH3* cells (54/55), and in 66% of *osh*Δ *OSH3 OSH6* cells (19/34). Bright internal fluorescence was observed in 25% of wild-type cells (11/44), 36% of *osh*Δ *OSH1 OSH3* cells (19/53), and in 76% of *osh*Δ *OSH3 OSH6* cells (26/34). (B) *osh*Δ P^{MET3}-*OSH2* (JRY6326) cells were cultured in the presence and absence of methionine and treated with filipin. In each series, left panels show cell morphology by DIC, and the right panels show the corresponding filipin fluorescence. Cells grown in the absence of methionine (–Met) displayed normal cell morphology and the pattern of filipin staining was comparable to that seen in wild-type cells. In the presence of methionine (+Met), Osh depleted *osh*Δ P^{MET3}-*OSH2* cells were larger in size, bud morphology and septation were defective, and the intensity of intracellular filipin fluorescence increased. (C) Filipin fluorescence was examined in wild-type cells (SEY6210), and in the temperature-sensitive mutants *osh*Δ *osh4-1* (CBY926), and *osh*Δ *osh4-2* (CBY928). At 23°C, more intracellular filipin fluorescence was observed in the *OSH* mutants compared with wild-type cells, and after 60 minutes at 37°C the intensity of intracellular fluorescence increased in mutant cells. In both (B) and (C), images of filipin fluorescence do not represent equal exposures; exposures were longer for wild-type cells.

visible. *OSH2* may be insufficient by itself to rescue the ergosterol distribution defect completely because *osh*Δ *OSH2* strains (where the wild-type *OSH2* is the sole *OSH* gene) exhibit many ergosterol-related defects (Beh et al., 2001). However, when *OSH2* expression was repressed in *osh*Δ P^{MET3}-*OSH2* cells, Osh protein depletion led to significant changes in morphology and sterol distribution in about half the cells (Fig. 9B). In these Osh-depleted cells, overall cell fluorescence increased due to an increase in cytoplasmic filipin fluorescence, and plasma membrane fluorescence decreased. In *osh*Δ *osh4(ts)* mutant strains at 37°C, filipin fluorescence at plasma membrane was comparable with wild-type cells but in these mutants significant cytoplasmic filipin staining was evident (Fig. 9C). These results indicated that *OSH* mutants affect intracellular sterol distribution.

ARV1 deletion caused endocytosis defects

To date, *ARV1* is the only gene reported other than the *OSH*s that affects sterol levels and distribution within yeast cells, without simply blocking sterol synthesis (Tinkelenberg et al., 2000). To determine if, like the *OSH*s, *ARV1* also plays a role in endocytosis, we evaluated lucifer yellow and FM4-64 uptake in *arv1*Δ cells. After a 60 minute incubation at 37°C, lucifer yellow uptake was reduced in *arv1*Δ cells relative to wild-type cells (Fig. 10A) indicating that fluid-phase endocytosis was defective. This defect was comparable to the internalization defect observed in *erg2*/*end11*Δ cells, which in addition to blocking ergosterol production also caused a pronounced endocytosis defect (Fig. 10A) (Munn et al., 1999). A modest defect was also observed for FM4-64 uptake in *arv1*Δ cells (Fig. 10B). The *arv1*Δ uptake defect was not as striking as that observed in *las17*Δ cells, but FM4-64 uptake was less efficient in the *arv1*Δ mutant than wild type. Thus, *ARV1* affected both sterol distribution and endocytosis.

To determine whether, like *OSH* mutants, the deletion of *ARV1* also had an effect on vacuole morphology, *arv1*Δ cells were stained for an extended period with FM4-64 to visualize vacuolar membranes. Under these conditions, FM4-64 was internalized and the dye-stained vacuole membranes revealed vacuolar fragmentation in *arv1*Δ cells (albeit minor compared with *erg2*Δ or *OSH* mutants; Fig. 10C). Despite these defects in vacuolar morphology, CPY processing and transport to the vacuole was unaffected in *arv1*Δ mutants when compared with wild-type cells (C.T.B., unpublished data). These results demonstrated that *ARV1* and *OSH* mutants shared similar defects, and suggested a connection between endocytosis, vacuolar morphology and the maintenance of sterol distribution.

Our results suggested a link between endocytosis and the maintenance of sterol distribution, so we examined whether all endocytosis mutants affect the cellular pattern of filipin/sterol

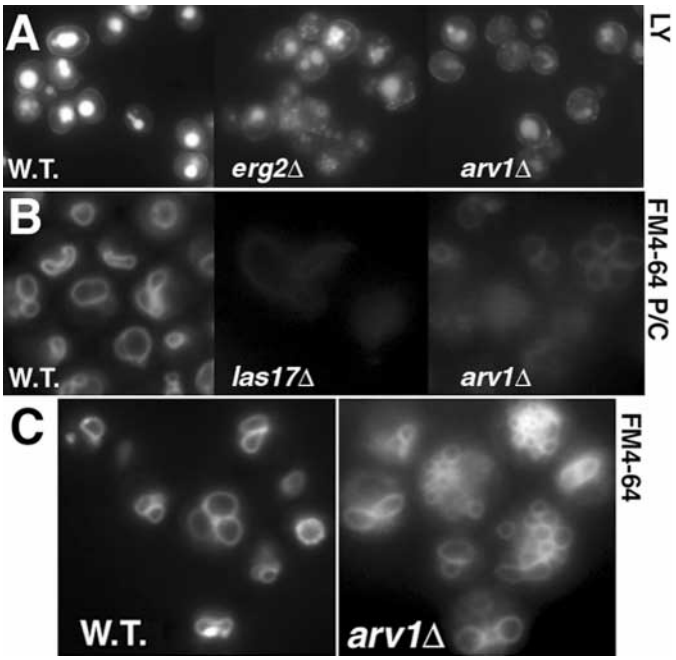

Fig. 10. *ARV1* deletion mutants exhibited endocytosis defects and fragmented vacuoles. (A) Lucifer yellow (LY) uptake and delivery to the vacuole was observed in wild-type (W.T.; CBY858), *erg2*Δ (CBY678) and *arv1*Δ (CBY994) cells grown at 30°C. In the wild-type strain, brightly stained vacuoles were observed in 92% of cells (154 out of 167 cells counted). In *erg2*Δ cells, only 2% of cells efficiently internalized lucifer yellow (1/50), and 0% of *arv1*Δ cells exhibited brightly staining vacuole or vacuolar fragments (0/72). (B) Wild-type (CBY858), *las17*Δ (CBY1024) and *arv1*Δ (CBY994) were treated with a short pulse of FM4-64 and then chased with fresh medium (FM4-64 P/C). Cells cultured at 30°C were viewed by fluorescence microscopy 30 minutes after the FM4-64 pulse/chase (P/C) and photographs were taken with equal exposures. (C) Wild-type (CBY858) and *arv1*Δ (CBY994) cells were cultured at 30°C in the presence of FM4-64 for 4 hours to label all vacuoles and vacuolar fragments uniformly (FM4-64). In *arv1*Δ cells, vacuolar fragmentation was evident in the proliferation of FM4-64 staining vacuole-derived rings.

staining. The essential gene *SLA2*/*END4* is involved in actin-dependent endocytosis (Raths et al., 1993; Holtzman et al., 1993). To determine whether *SLA2*/*END4* was required for the normal maintenance of sterol distribution, an *end4-1* endocytosis mutant was treated with filipin after incubation at 37°C, its nonpermissive growth temperature. The *end4-1* endocytosis mutant had no perceptible accumulation of internalized sterols and no change was detected at the plasma membrane (Fig. 11). These findings indicated that endocytosis defects per se do not cause sterol accumulation within yeast cells.

Actin is essential for yeast endocytosis (Kubler and Riezman, 1993; Munn et al., 1995), and many genes required for endocytosis affect actin assembly and dynamics (reviewed by D'Hondt et al., 2000). To examine whether *OSH*-associated endocytosis defects were actin dependent, we examined the actin cytoskeleton in *OSH* mutants. Wild-type and mutant cells were fixed and treated with rhodamine conjugated phalloidin, a fluorescent actin-binding probe. In both the *osh*Δ *osh4-1* and

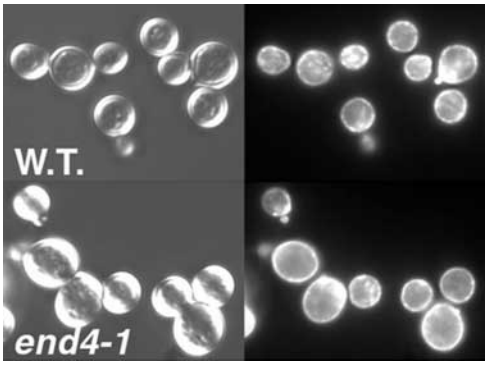

Fig. 11. Sterol lipid distribution was unaffected in *END4*/*SLA2* temperature-sensitive mutants. Leftmost panels show whole cell morphology by DIC, and the rightmost panels show the same cells stained with filipin. No intracellular accumulation of sterols was detectable by filipin staining in *sla2*/*end4-1* cells (RH286-1C) as compared with wild type (W.T.; W303-1A).

*osh*Δ *osh4-2* temperature-sensitive mutants at 37°C, the polarization of actin patches and the number and orientation of actin cables were comparable to wild-type cells (C.T.B., unpublished data). In addition, the actin cytoskeleton appeared unaffected in cells containing deletions of either *ERG2* or *ARV1* (C.T.B., unpublished data). Thus, the endocytosis defects associated with *erg2*Δ, *arv1*Δ, and temperature-sensitive *OSH* mutants were not manifested through any obvious effects on polymerized actin.

Discussion

From our previous studies of *OSH* mutants, we determined that the *OSH* genes perform many nonessential roles and that combined they share at least one essential function (Beh et al., 2001). In this paper we focused on the overlapping functions of all seven *OSH* genes, and found that the *OSH*s are involved in daughter cell budding, endocytosis and the maintenance of cellular sterol distribution. These findings imply a specific association between the intracellular transport of sterols and these other processes.

The *OSH* gene family and secretion

The deletion of *KES1*/*OSH4* suppresses the lethality associated with loss of *SEC14*, an essential gene required for Golgi vesicle budding, even though deletion of *OSH4* has no detectable effect on Golgi secretory transport (Fang et al., 1996). The implication is that *OSH4* does not facilitate Golgi secretion but rather acts as a repressor of *SEC14*-dependent Golgi transport. This suggests that *OSH4* overexpression might completely block Golgi secretion. Although the overexpression of any single *OSH* gene has no affect on growth, and thus no appreciable secretory defect (C.T.B., unpublished data), mammalian OSBPs expressed at high levels in yeast cause growth arrest and CPY-Golgi transport defects (Xu et al., 2001). These results indicate that the *OSH*s and OSBPs are negative regulators of Golgi secretion, although the purpose and mechanism is unclear.

Our results showed that the entire *OSH* gene family is

dispensable for the transport of several secretory proteins to the plasma membrane. Turning off the last remaining *OSH* gene, in cells that otherwise lacked all other *OSH*s, had little impact on Hsp150p, Gas1p, or invertase secretion to the plasma membrane. *OSH* inactivation also had insignificant effects on CPY transport to the vacuole, and CPY was not mis-sorted at the Golgi to the cell surface. These results indicated that the *OSH*s are not facilitators of exocytosis or trafficking from the Golgi to the vacuole, but do not preclude a role for the *OSH*s as negative regulators of secretion. Even so, our data indicated that the *OSH*s have other important roles in membrane trafficking and organelle morphology, which might be tied to Osh activities in affecting cellular lipid distribution.

The *OSH*s maintain sterol-lipid distribution and vacuolar integrity

The link between *OSH* mutants and sterols was established through the phenotypic analysis of all *OSH* deletion combinations (Jiang et al., 1994; Beh et al., 2001). Deletion of specific subsets of the *OSH* genes cause sterol-related defects affecting tryptophan uptake, ion transport and osmotic stress. In addition, many mutant combinations manifested altered sensitivities to the sterol-specific drugs lovastatin and nystatin. Consistent with these findings, in *OSH* mutants we observed defects in the cellular distribution of sterols. In addition to the intracellular accumulation of filipin-staining sterols, a decrease in plasma membrane filipin fluorescence was observed in some *OSH* mutants. Depletion of *OSH* function also caused lipid droplet accumulation. Following the gradual depletion of Osh proteins the level of cellular ergosterol increases 3.5-fold (Beh et al., 2001). Much of this excess ergosterol presumably resides in the lipid droplets observed by electron microscopy. Lipid droplets and filipin-stained sterols also accumulated after the rapid inactivation of *OSH* genes in *osh*Δ *osh4(ts)* cells at nonpermissive temperatures but total levels of cellular ergosterol were unchanged. Unlike gradual depletion of Osh proteins, rapid inactivation of *OSH*s in *osh*Δ *osh4(ts)* cells did not alter sterol composition or sterol levels when lipid extracts were compared with wild type (C.T.B. and L. Cool, unpublished). These findings indicated that defects in sterol distribution observed in *osh*Δ *osh4(ts)* cells were not the result of alterations in sterol synthesis. These results also suggested that the *OSH* gene family is not directly involved in sterol lipid metabolism but rather in maintaining ergosterol localization at the plasma membrane. During the limited period of growth that follows when Osh proteins are gradually removed, ergosterol mislocalization might perturb regulatory sensing of sterols in a particular membrane and sterol synthesis is thereby erroneously induced.

The disruption of cellular ergosterol distribution by Osh-depletion appears to have specific consequences on vacuolar morphology. In our experiments, regardless of how *OSH* function was turned off, the loss of all *OSH* function resulted in vacuolar fragmentation and collapse, and lipid droplets amassed within the fragmented remains of vacuoles. In wild type, lipid droplets were rarely seen within vacuoles, and ergosterol is not normally an abundant vacuolar lipid (Zinser et al., 1991). Substantial vacuolar fragmentation is also observed in ergosterol biosynthesis mutants (Munn et al., 1999; Kato and Wickner, 2001) in which the role of ergosterol in vacuolar integrity appears to be independent of vacuolar transport. Deletion mutants in the ergosterol biosynthetic genes *ERG2* or *ERG6* perturb vacuolar integrity, but neither deletion blocks CPY transport to the vacuole (Munn and Riezman, 1994). Likewise, in Osh-depleted cells, CPY delivery to the vacuole was essentially unaffected despite vacuolar collapse and fragmentation. Other vacuolar protein-sorting mutants also disrupt vacuole morphology and they can affect transport pathways other than that defined by CPY trafficking (Wickner and Haas, 2000). This raises the possibility that Osh proteins facilitate an aspect of vacuolar or endosomal trafficking other than that involving CPY. As discussed below, the *OSH*s are in fact necessary for endocytosis.

The *OSH*s are required for endocytic internalization

Inactivation of *OSH* function in a temperature-sensitive mutant disrupted lucifer yellow and FM4-64 uptake, and retarded Ste6p internalization from the plasma membrane. These results indicate that the *OSH*s are required for the internalization step of endocytosis. Similar to the *OSH* genes, we found that another gene that affects cellular ergosterol distribution, *ARV1*, also affected endocytosis. In *arv1*Δ cells, levels of plasma membrane sterols are reduced and sterols accumulate in intracellular membranes (Fig. 9B) (Tinkelenberg et al., 2000). We also observed endocytosis defects by lucifer yellow and FM4-64 uptake assays. Although the pattern of sterol accumulation within *arv1*Δ and Osh-depleted cells appeared to differ, the shared role in endocytosis suggests links between ergosterol and endocytic transport.

Model for the shared functions of the Osh protein family

The elimination of *OSH* function disrupted several cellular processes. Possibly the *OSH*s contribute to each of these processes independently, and the lethality of deleting all *OSH* genes is a consequence of a mixture of defects that cumulatively compromise growth. However this is unlikely given the rapid growth arrest observed after shifting *osh*Δ *osh4*(*ts*) cells to their nonpermissive temperature. The results suggest that the cellular processes affected by the *OSH*s are functionally integrated.

If there is a causal link between endocytosis, vacuole integrity and intracellular sterol distribution, then the primary defect caused by Osh protein depletion may be associated with any one of these functions. The evidence suggests that *OSH* inactivation blocks the recycling of ergosterol back to the cell surface and, in turn, this might explain all phenotypes generated by the loss of *OSH* function. This implies that plasma membrane sterols are required for endocytosis. Indeed, mutations in several genes required for ergosterol production are required for endocytosis; *ERG2*, which encodes a late-acting enzyme in the ergosterol biosynthetic pathway, was independently identified as the endocytosis gene *END11* (Munn and Riezman, 1994; Munn et al., 1999). Either ergosterol is required for endocytosis, or the precursor sterol that accumulates in *ERG2* mutants inhibits internalization. Our results are consistent with the model that ergosterol is necessary for endocytosis because both *ARV1* and *OSH* mutants perturb plasma membrane ergosterol and also disrupt endocytosis.

An alternative possibility is that the Osh proteins are themselves part of a complex directly involved in endocytosis. The rapid halt in endocytosis following *OSH* inactivation suggests that *OSH*s are directly involved. We did not detect sterol accumulation in an *end4-1* endocytosis mutant indicating that sterol trafficking defects are not ubiquitous aspects of endocytosis mutants. Thus, the *OSH* genes represent a specific class of lipid-related endocytosis genes.

What is the mechanism by which endocytosis is affected by changes in sterol levels or distribution? The interaction between actin complexes and the plasma membrane is important for yeast endocytosis (Kubler and Riezman, 1993; Munn et al., 1995) and may be sensitive to membrane lipid composition. In *ARV1*, *ERG2* or *OSH* mutants, however, the actin cytoskeleton and the distribution of actin patches on the plasma membrane appeared unaffected (C.T.B., unpublished data), indicating that the endocytosis defects observed in these mutants were actin independent. Alternatively, changes in plasma membrane sterol composition might disrupt endocytosis by altering membrane structure. In animal cells, the depletion of cholesterol from the plasma membrane alters the morphology of clathrin-coated pits and inhibits budding of clathrin-coated endocytic vesicles (Rodal et al., 1999; Subtil et al., 1999). Thus, *ARV1*, *ERG2* or *OSH* mutants, all of which affect plasma membrane lipid composition, might also affect the deformation of the plasma membrane required for endocytic vesicle formation. In this respect, the yeast *OSH*s appear to affect multiple transport processes by changing local membrane lipid composition.

Special thanks to members of the Drubin/Barnes laboratory for antibodies, strains and helpful suggestions, and to the Schekman laboratory for antibodies and strains. We gratefully acknowledge Robin Wright for technical advice and support, and Nancy Hawkins and Keith Kozminski for comments and suggestions on the manuscript. Thanks also to Tim Levine, Sean Munro and Robert Yang Hongyuan for sharing results before publication. This work was funded by a National Institutes of Health grant to J.R. (GM35827). C.T.B. was supported by Leukemia and Lymphoma Society Special Fellows grant #3042-00.

References

Adams, A., Gottsschling, D. E., Kaiser, C. A. and Stearns, T. (1997). *Methods in Yeast Genetics* (ed. M. M. Dickerson). Cold Spring, NY: Cold Spring Harbor Laboratory Press.

Bagnat, M., Keranen, S., Shevchenko, A., Shevchenko, A. and Simons, K. (2000). Lipid rafts function in biosynthetic delivery of proteins to the cell surface in yeast. *Proc. Natl. Acad. Sci. USA* **97**, 3254-3259.

Bankaitis, V. A., Aitken, J. R., Cleves, A. E. and Dowhan, W. (1990). An essential role for a phospholipid transfer protein in yeast Golgi function. *Nature* **347**, 561-562.

Beh, C. T., Cool, L., Phillips, J. and Rine, J. (2001). Overlapping functions of the yeast Oxysterol-binding protein homologues. *Genetics* **157**, 1117-1140.

Berkower, C., Loayza, D. and Michaelis, S. (1994). Metabolic instability and constitutive endocytosis of *STE6*, the a-factor transporter of *Saccharomyces cerevisiae*. *Mol. Biol. Cell* **5**, 1185-1198.

Berkower, C., Taglicht, D. and Michaelis, S. (1996). Functional and physical interactions between partial molecules of *STE6*, a yeast ATP-binding cassette protein. *J. Biol. Chem.* **271**, 22983-22989.

Brittman, R., Chen, W. C. and Blau, L. (1974). Stopped-flow kinetic and equilibrium studies of filipin 3 binding to sterols. *Biochemistry* **13**, 1374-1379.

Brown, M. S. and Goldstein, J. L. (1997). The SREBP pathway: regulation of cholesterol metabolism by proteolysis of a membrane-bound transcription factor. *Cell* **89**, 331-340.

Brown, M. S. and Goldstein, J. L. (1999). A proteolytic pathway that controls the cholesterol content of membranes, cells, and blood. *Proc. Natl. Acad. Sci. USA* **96**, 11041-11048.

Bryant, N. J. and Stevens, T. H. (1998). Vacuole biogenesis in *Saccharomyces cerevisiae*: protein transport pathways to the yeast vacuole. *Microbiol. Mol. Biol. Rev.* **62**, 230-247.

Dawson, P. A., van der Westhuyzen, D. R., Goldstein, J. L. and Brown, M. S. (1989). Purification of oxysterol binding protein from hamster liver cytosol. *J. Biol. Chem.* **264**, 9046-9052.

D'Hondt, K., Heese-Peck, A. and Riezman, H. (2000). Protein and lipid requirements for endocytosis. *Annu. Rev. Genet.* **34**, 255-295.

Fang, M., Kearns, B. G., Gedvilaite, A., Kagiwada, S., Kearns, M., Fung, M. K. and Bankaitis, V. A. (1996). Kes1p shares homology with human oxysterol binding protein and participates in a novel regulatory pathway for yeast Golgi-derived transport vesicle biogenesis. *EMBO J.* **15**, 6447-6459.

Gaber, R. F., Copple, D. M., Kennedy, B. K., Vidal, M. and Bard, M. (1989). The yeast gene *ERG6* is required for normal membrane function but is not essential for biosynthesis of the cell-cycle-sparking sterol. *Mol. Cell. Biol.* **9**, 3447-3456.

Gaynor, E. C. and Emr, S. D. (1997). COPI-independent anterograde transport: cargo-selective ER to Golgi protein transport in yeast COPI mutants. *J. Cell Biol.* **136**, 789-802.

Goffeau, A., Barrell, B. G., Bussey, H., Davis, R. W., Dujon, B., Feldmann, H., Galibert, F., Hoheisel, J. D., Jacq, C., Johnston, M. et al. (1996). Life with 6000 genes. *Science* **274**, 546-567.

Hardwick, K. G. and Pelham, H. R. (1994). *SED6* is identical to *ERG6*, and encodes a putative methyltransferase required for ergosterol synthesis. *Yeast* **10**, 265-269.

Heino, S., Lusa, S., Somerharju, P., Ehnholm, C., Olkkonen, V. M. and Ikonen, E. (2000). Dissecting the role of the Golgi complex and lipid rafts in biosynthetic transport of cholesterol to the cell surface. *Proc. Natl. Acad. Sci. USA* **97**, 8375-8380.

Holthuis, J. C., Nichols, B. J. and Pelham, H. R. (1998). The syntaxin Tlg1p mediates trafficking of chitin synthase III to polarized growth sites in yeast. *Mol. Biol. Cell* **9**, 3383-3397.

Holtzman, D. A., Yang, S. and Drubin, D. G. (1993). Synthetic-lethal interactions identify two novel genes, *SLA1* and *SLA2*, that control membrane cytoskeleton assembly in *Saccharomyces cerevisiae*. *J. Cell Biol.* **122**, 635-644.

Jiang, B., Brown, J. L., Sheraton, J., Fortin, N. and Bussey, H. (1994). A new family of yeast genes implicated in ergosterol synthesis is related to the human oxysterol binding protein. *Yeast* **10**, 341-353.

Kandutsch, A. A., Chen, H. W. and Heiniger, H. J. (1978). Biological activity of some oxygenated sterols. *Science* **201**, 498-501.

Kaplan, M. R. and Simoni, R. D. (1985). Transport of cholesterol from the endoplasmic reticulum to the plasma membrane. *J. Cell Biol.* **101**, 446-453.

Karpova, T. S., McNally, J. G., Moltz, S. L. and Cooper, J. A. (1998). Assembly and function of the actin cytoskeleton of yeast: relationships between cables and patches. *J. Cell Biol.* **142**, 1501-1517.

Kato, M. and Wickner, W. (2001). Ergosterol is required for the Sec18/ATP-dependent priming step of homotypic vacuole fusion. *EMBO J.* **20**, 4035-4040.

Kuchler, K., Sterne, R. E. and Thorner, J. (1989). *Saccharomyces cerevisiae STE6* gene product: a novel pathway for protein export in eukaryotic cells. *EMBO J.* **8**, 3973-3984.

Kubler, E. and Riezman, H. (1993). Actin and fimbrin are required for the internalization step of endocytosis in yeast. *EMBO J.* **12**, 2855-2862.

Levine, T. P. and Munro, S. (1998). The pleckstrin homology domain of oxysterol-binding protein recognizes a determinant specific to Golgi membranes. *Curr. Biol.* **8**, 729-739.

Levine, T. P. and Munro, S. (2001). Dual targeting of Osh1p, a yeast homologue of Oxysterol-binding protein, to both the Golgi and the nucleus-vacuole junction. *Mol. Biol. Cell* **12**, 1633-1644.

Li, R. (1997). Bee1, a yeast protein with homology to Wiscott-Aldrich syndrome protein, is critical for the assembly of cortical actin cytoskeleton. *J. Cell Biol.* **136**, 649-658.

Li, X., Rivas, M. P., Fang, M., Marchena, J., Mehrotra, B., Chaudhary, A., Fenf, L., Prestwich, G. D. and Bankaitis, V. A. (2002). Analysis of oxysterol binding protein homologue Kes1p function in regulation of Sec14p-dependent protein transport from the yeast Golgi complex. *J. Cell Biol.* **157**, 63-77.

Loewen, C. J. R., Roy, A. and Levine, T. P. (2003). A conserved ER targeting

motif in three families of lipid binding proteins and in Opi1p binds VAP. *EMBO J.* **22**, 2025-2035.

Munn, A. L. and Riezman, H. (1994). Endocytosis is required for the growth of vacuolar H(+)-ATPase-defective yeast: identification of six new *END* genes. *J. Cell Biol.* **127**, 373-386.

Munn, A. L., Stevenson, B. J., Geli, M. I. and Riezman, H. (1995). *end5*, *end6*, and *end7*: mutations that cause actin delocalization and block the internalization step of endocytosis in *Saccharomyces cerevisiae*. *Mol. Biol. Cell* **6**, 1721-1742.

Munn, A. L., Heese-Peck, A., Stevenson, B. J., Pichler, H. and Riezman, H. (1999). Specific sterols required for the internalization step of endocytosis in yeast. *Mol. Biol. Cell* **10**, 3943-3957.

Naqvi, S. N., Zahn, R., Mitchell, D. A., Stevenson, B. J. and Munn, A. L. (1998). The WASp homologue Las17p functions with the WIP homologue End5p/verprolin and is essential for endocytosis in yeast. *Curr. Biol*. **8**, 959-962.

Novick, P. and Schekman, R. (1979). Secretion and cell-surface growth are blocked in a temperature-sensitive mutant of *Saccharomyces cerevisiae*. *Proc. Natl. Acad. Sci. USA* **76**, 1858-1862.

Raths, S., Rohrer, J., Crausaz, F. and Riezman, H. (1993). *end3* and *end4*: two mutants defective in receptor-mediated and fluid-phase endocytosis in *Saccharomyces cerevisiae*. *J. Cell Biol.* **120**, 55-65.

Ridgway, N. D., Lagace, T. A., Cook, H. W. and Byers, D. M. (1998). Differential effects of sphingomyelin hydrolysis and cholesterol transport on oxysterol-binding protein phosphorylation and Golgi localization. *J. Biol. Chem*. **273**, 31621-31628.

Roberts, C. J., Raymond, C. K., Yamashiro, C. T. and Stevens, T. H. (1991). Methods for studying the yeast vacuole. *Methods Enzymol*. **194**, 644-661.

Robinson, J. S., Klionsky, D. J., Banta, L. M. and Emr, S. D. (1988). Protein sorting in *Saccharomyces cerevisiae*: isolation of mutants defective in the delivery and processing of multiple vacuolar hydrolases. *Mol. Cell. Biol.* **8**, 4936-4948.

Rodal, S. K., Skretting, G., Garred, O., Vilhardt, F., van Deurs, B. and Sandvig, K. (1999). Extraction of cholesterol with methyl-beta-cyclodextrin perturbs formation of clathrin-coated endocytic vesicles. *Mol. Biol. Cell* **10**, 961-974.

Rose, M. D., Misra, L. M. and Vogel, J. P. (1989). *KAR2*, a karyogamy gene, is the yeast homolog of the mammalian BiP/GRP78 gene. *Cell* **57**, 1211-1221.

Rothman, J. H., Howald, I. and Stevens, T. H. (1989). Characterization of genes required for protein sorting and vacuolar function in the yeast *Saccharomyces cerevisiae*. *EMBO J.* **8**, 2057-2065.

Russo, P., Kalkkinen, N., Sareneva, H., Paakkola, J. and Makarow, M. (1992). A heat shock gene from *Saccharomyces cerevisiae* encoding a secretory glycoprotein. *Proc. Natl. Acad. Sci. USA* **89**, 3671-3675.

Sambrook, J., Fritsch, E. F. and Maniatis, T. (ed.) (1989). *Molecular Cloning*, 2nd edn. Cold Spring, NY: Cold Spring Harbor Laboratory Press.

Schmalix, W. A. and Bandlow, W. (1994). *SWH1* from yeast encodes a candidate nuclear factor containing ankyrin repeats and showing homology to mammalian oxysterol-binding protein. *Biochim. Biophys. Acta. Mol. Cell Res.* **1219**, 205-210.

Severs, N. J. (1997). Cholesterol cytochemistry in cell biology and disease. *Subcell Biochem*. **28**, 477-505.

Sikorski, R. S. and Hieter, P. (1989). A system of shuttle vectors and yeast host strains designed for efficient manipulation of DNA in *Saccharomyces cerevisiae*. *Genetics* **122**, 19-27.

Storey, M. K., Byers, D. M., Cook, H. W. and Ridgway, N. D. (1998). Cholesterol regulates oxysterol binding protein (OSBP) phosphorylation and golgi localization in Chinese hamster ovary cells: correlation with stimulation of sphingomyelin synthesis by 25-hydroxycholesterol. *Biochem. J.* **336**, 247-256.

Subtil, A., Gaidarov, I., Kobylarz, K., Lampson, M. A., Keen, J. H. and McGraw, T. E. (1999). Acute cholesterol depletion inhibits clathrin-coated pit budding. *Proc. Natl. Acad. Sci. USA* **96**, 6775-6780.

Taylor, F. R., Saucier, S. E., Shown, E. P., Parish, E. J. and Kandutsch, A. A. (1984). Correlation between oxysterol binding to a cytosolic binding-protein and potency in the repression of hydroxymethylglutaryl coenzyme-A reductase. *J. Biol. Chem.* **259**, 12382-12387.

Tinkelenberg, A. H., Liu, Y., Alcantara, F., Khan, S., Guo, Z., Bard, M. and Sturley, S. L. (2000). Mutations in yeast *ARV1* alter intracellular sterol distribution and are complemented by human ARV1. *J. Biol. Chem.* **275**, 40667-40670.

Tomeo, M. E., Fenner, G., Tove, S. R. and Parks, L. W. (1992). Effect of sterol alterations on conjugation in *Saccharomyces cerevisiae*. *Yeast* **8**, 1015-1024.

Urbani, L. and Simoni, R. D. (1990). Cholesterol and vesicular stomatitis virus G protein take separate routes from the endoplasmic reticulum to the plasma membrane. *J. Biol. Chem.* **265**, 1919-1923.

Vida, T. A. and Emr, S. D. (1995). A new vital stain for visualizing vacuolar membrane dynamics and endocytosis in yeast. *J. Cell Biol*. **128**, 779-792.

Wach, A., Brachat, A., Pohlmann, R. and Philippsen, P. (1994). New heterologous modules for classical or PCR-based gene disruptions in *Saccharomyces cerevisiae*. *Yeast* **10**, 1793-1808.

Walker-Caprioglio, H. M., MacKenzie, J. M. and Parks, L. W. (1989). Antibodies to nystatin demonstrate polyene specificity and allow immunolabeling of sterols in *Saccharomyces cerevisiae*. *Antimicrob. Agents Chemother*. **33**, 2092-2095.

Welihinda, A. A., Beavis, A. D. and Trumbly, R. J. (1994). Mutations in *LIS1* (*ERG6*) gene confer increased sodium and lithium uptake in *Saccharomyces cerevisiae*. *Biochim. Biophys. Acta. Mol. Cell Res.* **1193**, 107-117.

Wendland, B., Steece, K. E. and Emr, S. D. (1999). Yeast epsins contain an essential N-terminal ENTH domain, bind clathrin and are required for endocytosis. *EMBO J.* **18**, 4383-4393.

Wickner, W. and Haas, A. (2000). Yeast vacuole fusion: a window on organelle trafficking mechanism. *Annu. Rev. Biochem*. **69**, 247-275.

Winzeler, E. A., Shoemaker, D. D., Astromoff, A., Liang, H., Anderson, K., Andre, B., Bangham, R., Benito, R., Boeke, J. D., Bussey, H. et al. (1999). Functional characterization of the *Saccharomyces cerevisiae* genome by gene deletion and parallel analysis. *Science* **285**, 901-906.

Woods, R. A. (1971). Nystatin-resistant mutants of yeast: alterations in sterol content. *J. Bacteriol*. **108**, 69-73.

Wright, R. (2000). Transmission electron microscopy of yeast. *Microsc. Res. Tech.* **51**, 496-510.

Wyles, J. P., McMaster, C. R. and Ridgway, N. D. (2002). Vesicle-associated membrane protein-associated protein-A (VAP-A) interacts with the oxysterol-binding protein to modify export from the endoplasmic reticulum. *J. Biol. Chem.* **277**, 29908-29918.

Xu, Y., Liu, Y., Ridgway, N. D. and McMaster, C. R. (2001). Novel members of the human oxysterol-binding protein family bind phospholipids and regulate vesicle transport. *J. Biol. Chem.* **276**, 18407-18414.

Zinser, E., Sperka-Gottlieb, C. D., Fasch, E. V., Kohlwein, S. D., Paltauf, F. and Daum, G. (1991). Phospholipid synthesis and lipid composition of subcellular membranes in the unicellular eukaryote *Saccharomyces cerevisiae*. *J. Bacteriol.* **173**, 2026-2034.